ResearchGate

See discussions, stats, and author profiles for this publication at: https://www.researchgate.net/publication/231633722

Brønsted Acid–Base Ionic Liquid as Proton-Conducting Nonaqueous Electrolytes

ARTICLE *in* THE JOURNAL OF PHYSICAL CHEMISTRY B · APRIL 2003

Impact Factor: 3.3 · DOI: 10.1021/jp022347p

CITATIONS
420

READS
51

6 AUTHORS, INCLUDING:

Md. Abu Bin Hasan Susan
University of Dhaka
73 PUBLICATIONS **4,246** CITATIONS
SEE PROFILE

Shigenori Mitsushima
Yokohama National University
125 PUBLICATIONS **2,957** CITATIONS
SEE PROFILE

Kikuko Hayamizu
University of Tsukuba
195 PUBLICATIONS **7,269** CITATIONS
SEE PROFILE

Masayoshi Watanabe
Yokohama National University
350 PUBLICATIONS **14,354** CITATIONS
SEE PROFILE

Available from: Masayoshi Watanabe
Retrieved on: 26 January 2016

Brønsted Acid−Base Ionic Liquids as Proton-Conducting Nonaqueous Electrolytes

Akihiro Noda,[†] Md. Abu Bin Hasan Susan,[†,‡] Kenji Kudo,[§] Shigenori Mitsushima,[§] Kikuko Hayamizu,[||] and Masayoshi Watanabe*[,†]

Departments of Chemistry and Biotechnology and of Energy and Safety Engineering, Yokohama National University, 79-5 Tokiwadai, Hodogaya-ku, Yokohama 240-8501, and National Institute of Advanced Industrial Science and Technology, AIST Tsukuba Central 5, Tsukuba, Ibaraki 305-8565, Japan

Received: October 31, 2002; In Final Form: February 11, 2003

A new series of Brønsted acid−base ionic liquids were derived from the controlled combination of a monoprotonic acid with an organic base under solvent-free conditions. Appropriate amounts of solid bis(trifluoromethanesulfonyl)amide (HTFSI) and solid imidazole (Im) were mixed at various molar ratios to have compositions varying from an equimolar salt to HTFSI- or Im-rich conditions. The mixture at equivalent molar ratio formed a protic neutral salt with a melting point of 73 °C, which was thermally stable at temperatures even above 300 °C. The melting points of other compositions were lower than those of the equimolar salt and Im or HTFSI, giving eutectics between the equimolar salt and HTFSI or Im. Some of the compositions with certain molar ratios of Im and HTFSI were liquid at room temperature. For Im excess compositions, the conductivity was found to increase with increasing Im mole fraction, and the ^{1}H NMR chemical shift of the proton attached to the nitrogen atom of Im was shifted to a lower magnetic field. On the contrary, the conductivity decreased with increasing HTFSI mole fraction, and the ^{1}H NMR chemical shift of the proton attached to the TFSI imide anion also shifted to a higher magnetic field. Self-diffusion coefficients, measured by pulsed-gradient spin−echo NMR (PGSE-NMR) methods in Im- or HTFSI-rich compositions, indicated that fast proton exchange reactions between the protonated Im cation and Im take place in excess Im. The proton conduction follows a combination of Grotthuss- and vehicle-type mechanisms. Direct current polarization measurements were used for the confirmation of proton conduction in Im-rich compositions. Furthermore, reduction of molecular oxygen could be observed at the interface between a Pt electrode and these ionic liquids. This introduces the Brønsted acid−base ionic liquid system as a new candidate for proton conductor such as a fuel cell electrolyte to operate under anhydrous conditions and at elevated temperature.

Introduction

Room temperature ionic liquids (RTILs) are liquids at ambient or even far below ambient temperature. These are comprised entirely of ions and are receiving an upsurge of interest in multidisciplinary areas for their unique physicochemical properties such as high thermal stability, negligible vapor pressure, relatively high ionic conductivity, and good electrochemical stability.

After the discovery of air- and water-stable RTILs by Cooper and Sullivan and Wilkes et al.,[1] many RTILs have been extensively explored, and their remarkable utility in diverse fields has been revealed. Our basic understanding of chemical reaction in solution using RTILs has taken a new turn in terms of selectivity, efficiency, and anomaly compared to molecular solvents such as water and organic solvents.[2] The need to develop environmentally benign reaction and separation processes has led to the potential use of RTILs as a green solvent for, inter alia, their immeasurably low vapor pressure and ease of handling.[3]

From the viewpoint of electrochemistry, RTILs themselves are ionic conductors and in many aspects excel typical ionic conductors for which the use of a solvent is a prerequisite to reveal ionic conductivity in electrochemical devices. Carlin et al. have constructed dual intercalating molten electrolyte batteries, wherein they used RTILs as an electrolyte.[4] Attempts have been made to widen the decomposition voltage to achieve excellent electromotive force and energy density.[5−8] The electric double-layer capacitance at the interface between RTILs and the electrode has been studied for the construction of the electric double-layer capacitor.[9−12] Consideration of durability and nonvolatility has also brought the RTILs into the forefront for wet devices of dye-sensitized solar cells using a photoelectrode with a Ru dye adsorbed on porous titania to achieve higher energy conversion efficiency.[13,14] Numerous efforts have also been made to use polymers with RTILs as ion-conducting polymer electrolytes. These include incorporation of RTILs in a polymer matrix such as a thermoplastic polymer[15] or a perfluoro ion exchange membrane,[16] polymerization of a vinyl monomer in RTILs,[17] and fixing of the cation or anion structure in the polymer segments.[18]

In terms of the structure of RTILs, reports focus on a combination of new anions and cations to prepare novel ionic liquids,[1a,6−8,19−44] and studies on their physical and chemical properties[45−69] and dependence of the melting point, viscosity, solubility to a solvent, and ionic conductivity on the alkyl chain length in the cation.[6−8,23−24,27−28,35,37,40,42−44] Most of the RTILs

* To whom correspondence should be addressed. E-mail: mwatanab@ynu.ac.jp. Fax: +81-45-339-3955.

[†] Department of Chemistry and Biotechnology, Yokohama National University.

[‡] Permanent address: Department of Chemistry, University of Dhaka, Dhaka 1000, Bangladesh.

[§] Department of Safety Engineering, Yokohama National University.

[||] National Institute of Advanced Industrial Science and Technology.

10.1021/jp022347p CCC: $25.00 © 2003 American Chemical Society
Published on Web 04/04/2003

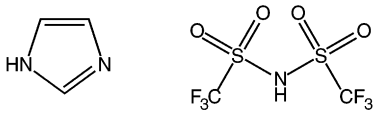

Figure 1. Molecular structures of Im and HTFSI.

in these studies are aprotic and are chemically and electrochemically stable, while only few reports deal with protic RTILs to confirm changes in physical properties with control of the alkyl chain from a minimum to varying lengths.[2c,27,29,36,70] However, a Brønsted acid−base protic ionic liquid has a long history since the first discovery of a protic ionic liquid, EtH_3NNO_3,[71] and the area is still emerging.

The use of an amine base−protonic acid system as a proton conductor in nonaqueous states was earlier reported by Takahashi et al. wherein they showed that the complexes of triethylenediamine or hexamethylenetriamine with H_2SO_4 exhibit proton conductivity.[72] Attention also has recently focused on the fixing of a basic site in a polymer chain to obtain a thermostable polymer, and to blend it with a protonic acid with high proton dissociation ability such as polybenzimidazole and H_3PO_4,[73] and other systems[74] to investigate the proton conduction characteristics and thermal stability. The conductivity in a zirconium phosphate complex was also found to be improved by addition of imidazole.[75] In contrast to these systems, where a protonic acid acts as a proton donor, an acceptor, and a carrier, Kreuer et al. introduced imidazole or pyrazole as a proton carrier.[76] The observation that conductivity is remarkably changed with a change in composition in the systems of imidazole or pyrazole and H_2SO_4 opened a new route and attracted significant attention among the researchers. They propounded one approach to realize fast proton conduction under an anhydrous condition using protic amphoteric materials with large self-dissociation ability as a proton conductor.[76,77] The concept has been applied in a recent paper to imidazole dimers with poly(ethylene oxide) chains as a flexible spacer, and the proton conduction behavior of the systems was analyzed.[78]

Imidazole derivatives and some other amine compounds neutralized by a strong monoprotonic acid such as HBF_4,[27,29,70] HPF_6,[2c] and HTFSI[36] aqueous solutions form neutral salts, which melt near room temperature. Analyses of the melting point, viscosity, and ionic conduction behavior of such ionic liquids have been reported, but no information on the proton conduction is available. Moreover, the combination of simple imidazole with a monobasic acid under solvent-free conditions was reported only for the sulfanilic acid system,[76] and the behavior with a superacid still remains unveiled. This prompted us to study the system of a monoprotonic acid, bis(trifluoromethanesulfonyl)amide (HTFSI) and imidazole under anhydrous conditions. The composition was widely varied, and the melting point, ionic conductivity, and proton conduction behavior were examined. This work deals with proton acid−base chemistry and proton transport behavior under anhydrous conditions, and is directed to electrolyte invention under nonhumidifying conditions for a new mesothermal fuel cell.

Experimental Section

Materials. HTFSI (Morita Chemical Industries, 99.8%) was used as received. Imidazole (Im) (Junsei Chemical Co. Ltd., >99%) was dried under vacuum at 60 °C for 24 h before use. Chemical structures of HTFSI and Im are shown in Figure 1. Appropriate amounts of HTFSI and Im maintaining defined molar ratios were mixed and heated above the respective melting points. All the samples were handled and stored in an argon atmosphere glovebox (VAC, $[O_2] < 1$ ppm, $[H_2O] < 1$ ppm).

Thermal Property. Differential scanning calorimetry (DSC) was carried out with a Seiko Instruments differential scanning calorimeter 220C under a N_2 atmosphere. The calibration of temperature and heat capacity was made by using cyclohexane, indium, and tin as standards. The samples for DSC measurements were tightly sealed by using Al pans in a glovebox. Thermograms were recorded during cooling (+30 to −150 °C) scans, followed by heating (−150 to +250 °C) at a cooling and heating rate of 10 °C min^{-1}. The glass transition temperature (T_g, onset of the heat capacity change), crystallization temperature (T_c, onset of the exotherm peak), melting temperature (T_m, onset of the endotherm peak), and melting temperature of the eutectic mixture (T_e, onset of the endotherm peak) were determined from DSC thermograms during the heating scans. High-temperature stabilities for the samples were measured on a Seiko Instruments thermogravimetry/differential thermal analyzer 6200 from 30 to 450 °C at a heating rate of 10 °C min^{-1} under an air atmosphere with open Al pans. Calcium oxalate monohydrate, $CaC_2O_4 \cdot H_2O$, was used as the standard for the calibration of the thermogravimetric changes.

Ionic Conductivity. The ionic conductivity was determined using the complex impedance method in the temperature range of 30−130 °C (ESPEC temperature chamber SU-220). The samples were thermally equilibrated at each temperature for at least 1 h prior to the measurements. In the cases of HTFSI-rich compositions, the measurements were carried out only at temperatures below the decomposition temperature. The electrolytes were filled up between two mirror-finished stainless steel electrodes using a Teflon ring spacer in a constant-volume cylindrical cell (7 mm electrode diameter and 2 mm fixed electrode distance), and sealed in a Teflon container in the glovebox. The cell constant, determined by 0.1 M KCl standard solution (Kanto Kagaku), was 0.52 cm^{-1} at 30 °C. The experiments were carried out with a computer-interfaced Hewlett-Packard 4192A LF impedance analyzer over the frequency range from 5 to 13 MHz.

^{1}H NMR Chemical Shift. The FT-NMR spectra were obtained on a spectrometer (JEOL EX-270) at 270 MHz for ^{1}H. Chemical shifts were determined by using a double tube (SC-002, Shigemi Co. Ltd.; inner tube, 3 mm i.d., 4.1 mm o.d.; outer tube, 4.2 mm i.d., 4.965 mm o.d.) with the sample in the inner tube and deuterium oxide containing 1 wt % 2,2-dimethyl-2-silapentane-5-sulfonic acid, sodium salt (DSS) as standard (Aldrich Chemical Co.) in the outer tube. All measurements were conducted at 22 °C.

Self-Diffusion Coefficient. The pulsed-gradient spin−echo NMR (PGSE-NMR) measurements were made by using a JEOL GSH-200 spectrometer with a 4.7 T wide-bore superconducting magnet, which was controlled by a TecMAG Galaxy system equipped with JEOL pulse field gradient probes and a current amplifier.[60,79] The ^{19}F and ^{1}H spectra were measured with a ^{19}F/^{1}H probe. Each of the composition samples was placed in a 5 mm (o.d.) NMR microtube (BMS-005J, Shigemi Co. Ltd.) to a height of 5 mm. The absolute magnitude of the field gradient was calibrated against the value of the self-diffusion coefficient of water at 30 °C. After a 90° pulse and longitudinal relaxation time (T_1) and transversal relaxation time (T_2) measurements, the self-diffusion coefficients were measured using the simple Hahn spin−echo (i.e., $90° - \tau - 180° - \tau -$ acq) sequence incorporating a gradient pulse in each τ period. The echo signal

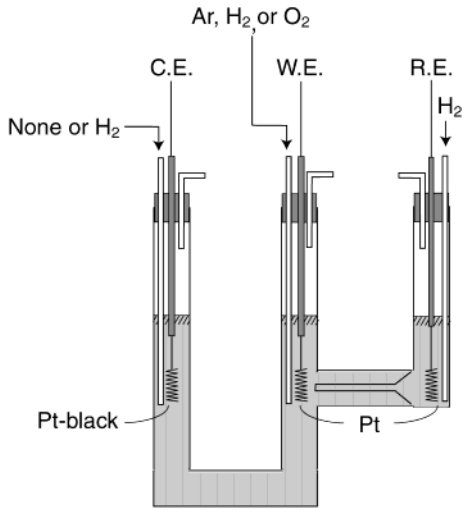

Figure 2. Schematic diagram of the two-compartment cell for the investigation of electrochemical polarization.

attenuation, E, is related to the experimental parameters by[80]

$$E = \exp(-\gamma^2 g^2 D\delta^2(\Delta - \delta/3)) \quad (1)$$

where γ is the gyromagnetic ratio, g is the amplitude of the gradient pulses of the duration δ, and Δ is the interval between the leading edges of the gradient pulses. In the present experiments, the g value used was constant (3.50 T m^{-1}), δ was in the range of 0−3 ms, and the value of Δ was 30 ms. A recycle delay sufficient for allowing full relaxation (i.e., $>5T_1$) was used between each transition. The measurements of the self-diffusion coefficients for the proton, which was attached to the nitrogen atom and bonded to the carbon atom of Im and/or attached to the nitrogen atom of TFSI, and the fluorine atom of TFSI in each electrolyte, were made by using the ^1H and ^{19}F nuclei, respectively. The measurements were carried out at 30 °C.

Electrochemical Polarization. Direct current polarization was performed at 25 °C using a U-shaped glass tube with two Pt-wire electrodes (proton pump cell). H_2 or N_2 gas was introduced at the vicinity of the anode by means of a Teflon tube. Cyclic voltammetry was performed at 80 °C for [Im]/[HTFSI] = 85/15 and 7/3 compositions using a two-compartment glass cell under a dry Ar, H_2, or O_2 gas bubbling atmosphere (Figure 2). The working and reference electrodes were coil-shaped Pt wires (0.5 mm diameter, 4.5 cm length), and the counter electrode was a coil-shaped Pt-black wire. The Pt wire in a H_2 atmosphere for all the experiments worked as a reversible hydrogen electrode (RHE). For power generation (fuel cell) experiments, the working electrode was set under an O_2 gas bubbling atmosphere, while the counter electrode was under a H_2 gas bubbling atmosphere. The electrodes were treated by repetitious cathodic and anodic polarization in 2 M H_2SO_4 solution before every experiment. The surface area of the working electrode was estimated from the H_2 adsorption−desorption value of 1 M H_2SO_4 solution at 30 °C in an Ar atmosphere. In all of the experiments, the electrodes and gas tubes were mounted in the glass cells using a Swagelok tube connector. The electrochemical control was accomplished using a Solartron electrochemical interface (model 1287). All data were collected and analyzed on a PC with commercial CorrWare 2 and CorrView softwares (Scribner Associates Inc.), respectively. The temperature was regulated by using a constant-temperature chamber (Yashima, BX-10).

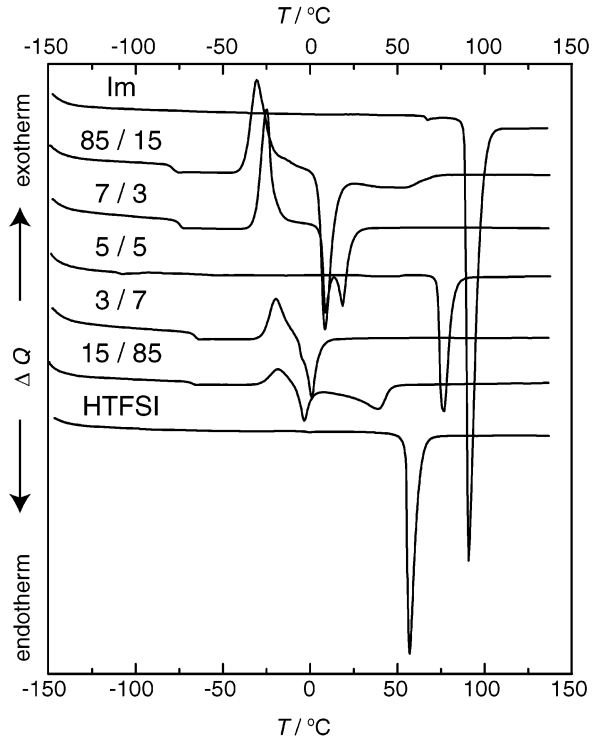

Figure 3. DSC thermograms of Im/HTFSI compositions with different mole fractions of Im. The heating rate is 10 °C min^{-1}.

TABLE 1: Thermal Properties for Im/HTFSI Compositions

[Im]/[HTFSI]	T_g/°C[a]	T_c/°C[a]	T_e/°C[a]	T_m/°C[a]	T_d/°C[b]
10/0				89	147
9/1	−89	−34	6	38	not measured
85/15	−82	−39	4	25	169
8/2	−81	−33		6 (T_e)	186
75/25	−80	−27		7 (T_e)	201
7/3	−77	−31	6	16	212
6/4	−82	−35	7	33	326
5/5				73	379
4/6	−69	−38	−7	25	126
3/7	−68	−27		−6 (T_e)	113
25/75	−70				107
2/8	−81				102
15/85	−70	−28	−8	20	not measured
1/9	−67	−38	−7	43	not measured
0/10				55	not measured

[a] Onset temperatures of a heat capacity change (glass transition temperature, T_g), an exotherm peak (crystallization temperature, T_c), and an endotherm peak, either one (melting temperature, T_m) or two (melting temperature of eutectic mixture, T_e and T_m) during heating scan from −150 °C by using differential scanning calorimetry. [b] Temperature of 10% weight loss heating scan from room temperature by using thermogravimetry.

Results and Discussion

Thermal Behavior. Thermal properties for the Im/HTFSI compositions were studied using DSC. Figure 3 shows the DSC thermograms at the heating scans for the various compositions of the Im−HTFSI system. The single endotherm peak corresponds to T_m for the neat Im and HTFSI and the equimolar salt. The thermograms also showed T_g, T_c, T_e, and T_m, successively, for other compositions. The DSC results and the thermal stability determined by thermogravimetry/differential thermal analysis (TG/DTA) measurements are summarized in Table 1. Im, HTFSI, and the 5:5 composition of Im−HTFSI are all solid at room temperature with melting points, T_m, os 89,[81] 55,[82] and 73 °C, respectively. T_m varied with composition,

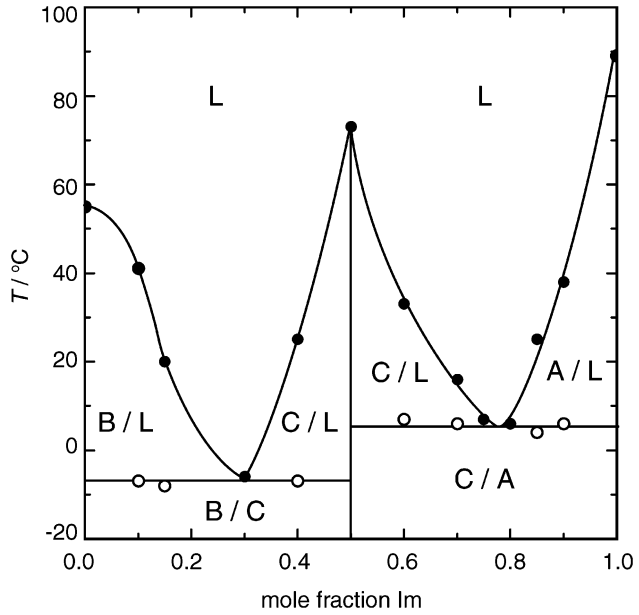

Figure 4. Phase diagram of the system Im−HTFSI. A, B, C, and L refer to Im, HTFSI, Im/HTFSI equimolar salt, and liquid, respectively. HFSI-rich composition with the mole fraction of Im as 0.20 does not crystallize and form a homogeneous glass.

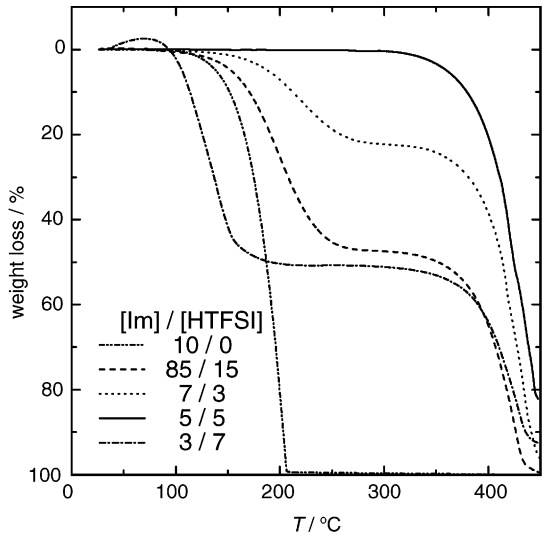

Figure 5. TG curves of Im/HTFSI compositions with different mole fractions of Im. The heating rate is 10 °C min^{-1}.

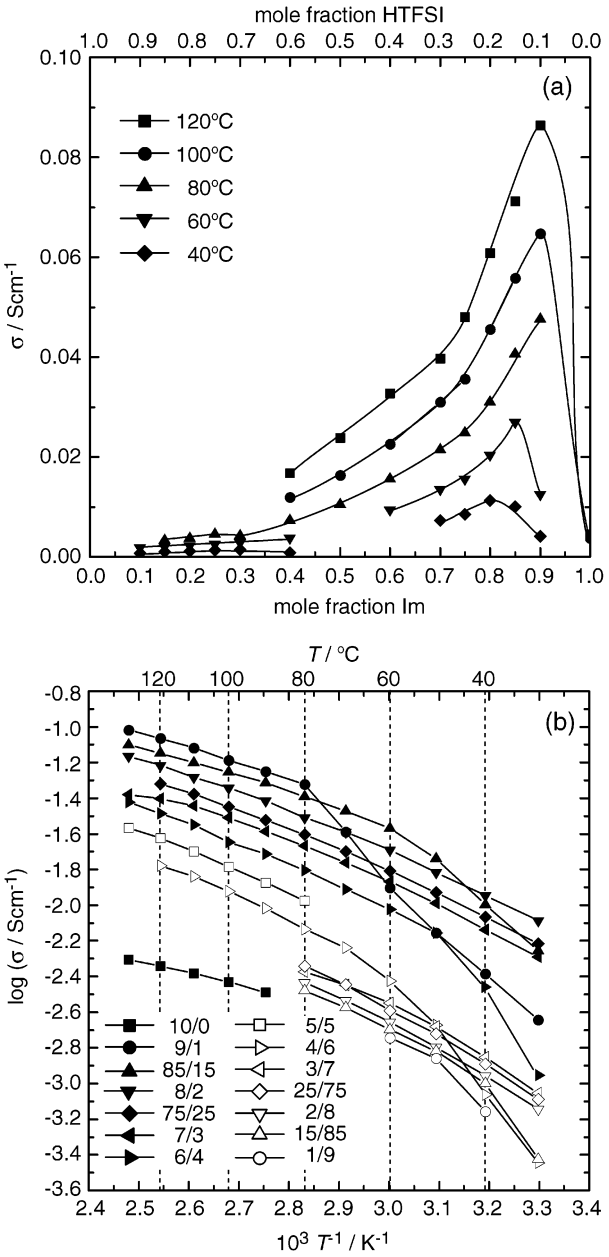

Figure 6. Ionic conductivity as a function of (a) the mole fraction of Im and (b) temperature for the system Im−HTFSI.

whereas T_e remained unchanged for either Im- or HTFSI-rich compositions. There is a eutectic at ca. −6 °C for compositions between pure HTFSI and the equimolar salt and also between the equimolar salt and Im at ca. 6 °C. A phase diagram of the Im−HTFSI system is depicted in Figure 4. This is a typical phase diagram of binary mixtures (HTFSI and salt, salt and Im), where they form homogeneous liquids but are phase-separated in the solid states. Some of the compositions with certain molar ratios of Im and HTFSI were liquid at room temperature. Resembling the thermal behavior of typical Lewis acid−base ionic liquids,[83] T_m changed with a change in the mole fraction in the Im−HTFSI system. At some HTFSI-rich compositions ([Im]/[HTFSI] = 25/75 and 2/8), the mixtures do not crystallize and form homogeneous glasses (Table 1).

Figure 5 shows the thermogravimetric changes of some of the compositions. The TG curve for the 5:5 mixture shows a one-step weight loss process with the detection of change only above 300 °C indicating high thermal stability. This is further evidence of the formation of a protic neutral salt, i.e., imidazolium bis(trifluoromethanesulfonyl)imide (HImTFSI), from the equimolar mixture of Im and HTFSI melting at 73 °C. The TG curves for Im and HTFSI excess compositions, on the contrary, show two-step weight loss processes, the initial losses corresponding to the excess amount of Im and HTFSI in the system.

Proton-Transport Mechanism Proposed from Conductivity Measurements. The composition dependence of ionic conductivity at certain temperatures is shown in Figure 6a. The ionic conductivity above the melting point increases with increasing Im mole fraction with a sharp decrease for neat Im. This is in good agreement with Kreuer et al. in excess Im, but sharply contrasts with the protonic acid excess compositions (vide infra).[76] Since the number of ion carriers, HIm^+ and $TFSI^-$, is maximum at the equimolar composition, the increase in ionic conductivity with increasing Im mole fraction indicates

the enhanced ionic mobility. Kreuer et al. have already pointed out that proton transport between the protonated Im (HIm^+) and neat Im (the proton defects, i.e., vacant nitrogen site of Im) plays an important role for intermolecular proton transfer, and at an optimum composition enhances the proton conduction.[76] Thus, the conductivity is due not only to ionic species such as HIm^+ and $TFSI^-$, but also to intermolecular proton transfer. The proton conduction is feasible even for neat Im for its characteristic proton self-dissociation, in other words, protolysis or ionization.[76−77,81,84] The HIm^+ species in neat Im accelerates a proton transfer dominantly via the Grotthuss mechanism in Im excess compositions.[76] The HIm^+ and $TFSI^-$ species also considerably influence the conduction behavior as the ionic transport above the melting point of the system. The proton conduction, therefore, seems to follow a combination of Grotthuss- and vehicle-type mechanisms,[85,86] with the contribution from the particular mechanism being a variable of the composition. The increase in the Im mole fraction from the equimolar salt renders dominant conducting properties to change from the vehicle to the Grotthuss mechanism.[76]

In the composition range of our measurements, the conductivity decreases with increasing HTFSI mole fraction from the equimolar salt. The high sublimability and volatility of HTFSI make it diffucult for the conductivity measurement to have the value of the ionic conductivity of neat HTFSI. However, it is likely that the conductivity increases rapidly upon addition of Im to pure HTFSI. The fact that the conductivity from the equimolar salt to an HTFSI-rich composition has a decreasing trend arises mainly from the decrease of ion carriers, HIm^+ and $TFSI^-$, and the small proton transference ability through the TFSI anion. Despite strong acidity,[82,87] HTFSI, in the HTFSI-rich compositions, exists mainly in the molecular state. HTFSI is a monoprotonic−monobasic acid with no intermolecular proton transference ability, and due to the extremely small basicity and low nucleophilicity,[25,56] the proton defects of the TFSI anion decrease with increasing HTFSI composition.

The temperature dependence of ionic conductivity is shown as Arrhenius plots in Figure 6b. The compositions exhibit ionic conductivity below T_m with an apparent inflection for the transition from a homogeneous liquid to a liquid−solid mixture. Above T_m, the temperature dependence of the ionic conductivity shows a gradual increase with increasing HTFSI concentration. The negatively charged species, $TFSI^-$, hinders the intermolecular proton transfer through Im and HIm^+. Whether the temperature dependence of the Im−HTFSI sytem obeys the Arrhenius formula or the VTF equation remains dubious. We speculate that a change from the VTF[1a,10c,23,45,60] to Arrhenius[81] type is likely with a change in the Im content in the compositions for the variety of conducting species and the conduction mechanism, as discussed above.

Evidence of Proton Transport from the ^{1}H NMR Chemical Shift and Self-Diffusion Coefficient. The electron density on ^{1}H and the extent of hydrogen bonding affects the NMR chemical shift of a proton. The use of a double NMR tube prevented mixing of a sample and D_2O containing 1 wt % DSS and allowed us to carry out ^{1}H NMR measurements of the neat Im/HTFSI compositions. The ^{1}H NMR spectra are shown in Figure 7 (a, [Im]/[HTFSI] = 75/25; b, [Im]/[HTFSI] = 25/75), and the mole fraction dependencies of chemical shifts are depicted in Figure 8. The sharp ^{1}H signals for both Im- and HTFSI-rich compositions have been assigned to the respective protons shown in Figure 7. The number of signals in the Im-rich composition was three, while it was four in the HTFSI-rich composition. Since proton exchange between Im and the

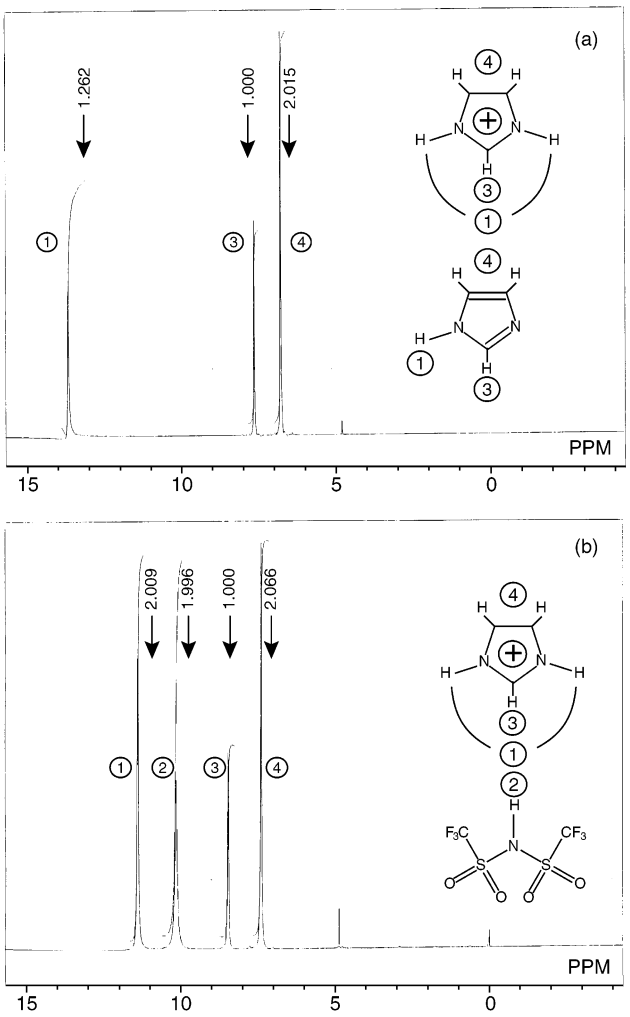

Figure 7. ^{1}H NMR spectra relative to external DSS in D_2O solvent for the (a) Im-rich composition ([Im]/[HTFSI] = 75/25) and (b) HTFSI-rich composition ([Im]/[HTFSI] = 25/75) at 22 °C using a double tube.

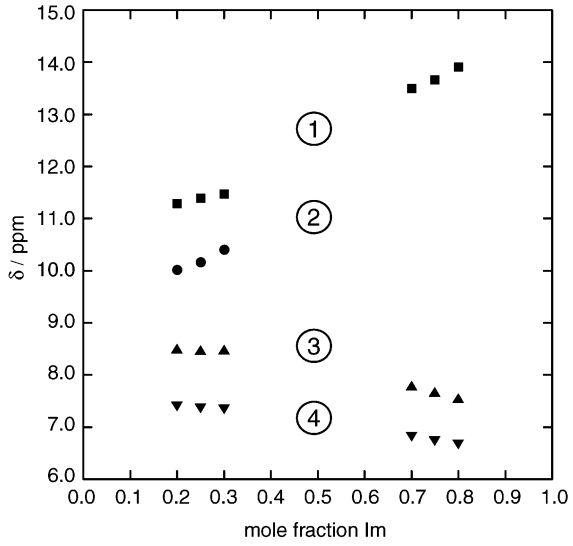

Figure 8. ^{1}H NMR chemical shift as a function of composition of the system Im−HTFSI.

HIm^+ is extremely fast ($>10^9$ s^{-1}) in Im excess compositions, both species cannot be separated by NMR. Furthermore, with increasing Im mole fraction in the Im-rich composition, the number of hydrogen-bonded species increases, as can be judged

TABLE 2: Diffusion Coefficient for Im/HTFSI Compositions at 30 °C

	$D/10^{-7}$ cm^2 s^{-1}						
[Im]/[HTFSI]	Im(^{1}H)[a]	HIm(^{1}H)[b]	TSFI(^{19}F)[c]	H-TFSI(^{1}H)[d]	$D_{H+}/10^{-7}$ cm^2 s^{-1}	$D_{H+}/D_{Im(1H)}$	$D_{H+}/D_{TFSI(19F)}$
8/2	5.7	6.3	3.7		8.1	1.4	
7/3	3.8	4.1	2.5		4.5	1.2	
3/7	1.2	1.2	1.3	1.4	1.5		1.2
2/8	1.4	1.4	1.7	1.9	2.0		1.2

[a] ^{1}H bonded to carbon atoms of imidazole. [b] ^{1}H attached to the nitrogen atom of imidazole. [c] ^{19}F of TSFI. [d] ^{1}H of HTFSI.

from a shift to lower magnetic field of the HIm^+ proton (Figure 8), because of enhancement of the vacant nitrogen site of Im, i.e., proton defects, and the multicoordination ability of Im to HIm^+. All Im molecules are protonated in HTFSI excess compositions, and the chemical shift due to excess HTFSI appears at a magnetic field higher than that of the proton attached to the nitrogen atom of Im. From the correlation of chemical shift with electron density, it is apparent that the ^{1}H of HIm^+, which comes from the proton source HTFSI, has less electron density, and thereby higher acidity, than the ^{1}H of the original HTFSI. With increasing HTFSI concentration in the HTFSI-rich composition, the chemical shift of the HTFSI ^{1}H is directed to a higher field. Only the TFSI anion can act as a proton acceptor, and the number of proton defects decreases with increasing HTFSI concentration. The other signals for the ^{1}H atoms bonded to the carbon atom of the Im ring also show interesting behavior. Whereas there is no notable difference in chemical shifts in HTFSI excess conditions, they exhibit a higher shift in excess Im. The positive charge on the ring structure, which is responsible for the constancy or shifting of the chemical shifts, decreases with an increase in the Im content in Im excess compositions due to delocalization of H^+ between HIm^+ and Im.

To investigate the diffusion behavior and separating the intermolecular proton transfer from the matrixes, we conducted PGSE-NMR measurements of some of the compositions in both Im- and HTFSI-rich conditions. Three and four different diffusion nuclei are confirmed in the Im- and HTFSI-rich compositions, respectively. The measured self-diffusion coefficients are summarized in Table 2. The self-diffusion coefficient of the ^{1}H attached to the nitrogen atom of Im ($D_{HIm(1H)}$, assignment number 1 in Figure 7) differs from the Im diffusion coefficient ($D_{Im(1H)}$, assignment numbers 3 and 4 in Figure 7) in Im excess conditions. It is worthwhile to note the difference in the diffusion coefficients, while the order is the same since the diffusion time Δ is 30 ms in the measurements and the mean squared displacement ($(2D\Delta)^{1/2}$) is of micrometer order. The obtained diffusion coefficients are average values on that scale. However, the difference indicates the existence of a fast intermolecular proton transfer, and thus, the diffusion coefficient of HIm(^{1}H) is larger than the matrix diffusion coefficient of Im(^{1}H). The experimental HIm(^{1}H) diffusion coefficients include both protonated Im (HIm^+) and neat Im. Thus, the H^+ diffusion coefficient (D_{H+}) is calculated by the experimental diffusion coefficients (Im(^{1}H) and HIm(^{1}H)) with the component mole fraction,[88] assuming that the ^{1}H self-diffusion coefficient ($D_{HIm(1H)}$) is the weight average of a normal diffusion process, $D_{Im(1H)}$, and a fast H^+ diffusion process, D_{H+}:

$$D_{HIm(1H)} = xD_{H+} + (1 - x)D_{Im(1H)} \quad (2)$$

where x is the mole fraction of imidazolium in the total base. In HTFSI-rich compositions, the self-diffusion coefficient of the ^{1}H of HTFSI ($D_{HTFSI(1H)}$, assignment number 2 in Figure 7) is also slightly larger than that of ^{19}F of TFSI ($D_{TFSI(19F)}$). The $D_{HTFSI(1H)}$ is also considered to be the weight average of $D_{TFSI(19F)}$ and D_{H+}, as follows:

$$D_{HTFSI(1H)} = yD_{H+} + (1 - y)D_{TFSI(19F)} \quad (3)$$

where y is the mole fraction of HTFSI in the total acid. The D_{H+} values in Im excess and HTFSI excess compositions are shown in Table 2. In Im excess conditions, the ratios of the estimated fast diffusion coefficient to the measured one, which is assigned to the Im matrix diffusion, for the mole fractions studied are 1.4 and 1.2, and the higher value of the ratio with higher Im content corresponds to a lower magnetic field shift of the ^{1}H NMR spectra and increasing conductivity. If the $D_{Im(1H)}$ is assumed to be the same as the self-diffusion coefficient of the imidazolium cation (vehicle mechanism), proton transfer by the intermolecular proton exchange process (Grotthuss mechanism) enhances D_{H+} by factors of 1.4 and 1.2 for [Im]/[HTFSI] = 8/2 and 7/3 compositions, respectively. Furthermore, the apparent ^{1}H transference numbers compared to TFSI(^{19}F) are 69% and 64% for the Im-rich compositions, the dominant conductive species being the proton transport in Figure 6. In HTFSI excess compositions, Im(^{1}H) and HIm(^{1}H) diffusion coefficients show identical values. All Im molecules are protonated in concentration equal to that of HTFSI as discussed above, and the proton is not exchanged with any components but is transported with the matrix Im following the vehicle mechanism. On the contrary, the diffusion coefficient of ^{1}H attached to the TFSI anion (H−TFSI(^{1}H)) is larger than that of the matrix TFSI anion (TFSI(^{19}F)). The H^+ diffusion coefficients (D_{H+}) and the compared ratios with TFSI(^{19}F) are shown in Table 2. The possibility of proton exchange through the TFSI anion is considered, but the conductivity decrease and higher field chemical shift of ^{1}H attached to TFSI with increasing HTFSI composition (Figures 6 and 8) suggest that the decrease in the number of ionic species rather than the proton diffusivity mainly affects the conducting behavior and the decline of intermolecular proton transport is correlated with the chemical shift. The proton associates with the TFSI anion, and the excess HTFSI in the system exists dominantly as the associated molecular HTFSI. The TFSI(^{19}F) diffusion coefficients are detected by the ^{19}F nucleus; thus, these diffusion coefficients contain both the TFSI anion and HTFSI molecular components. This might be the most probable reason for the larger diffusion coefficient for the molecular HTFSI(^{1}H) than that of the anionic TFSI(^{19}F).

Decisive Feature of Proton Transport from Electrochemical Polarization. To corroborate the protonic conduction electrochemically in base-rich Im/HTFSI compositions, a simple direct current polarization experiment (proton pump) was conducted. Figure 9 shows the current−voltage characteristics of the proton pump cell, where the anode was under a H_2 or N_2 bubbling atmosphere. The current detected under a N_2 atmosphere was quite low, whereas a very noticeable change could be distinguished upon the change of the atmosphere to a H_2 gas atmosphere, resulting in the observation of much higher

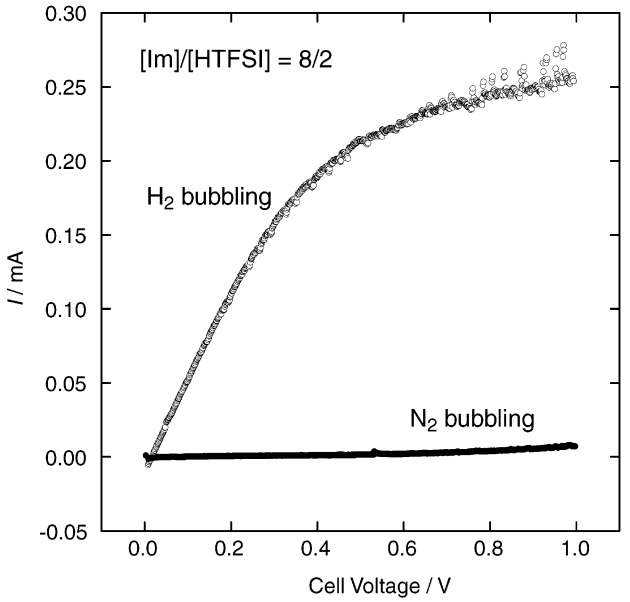

Figure 9. Relationship between cell voltage and detected direct current at 25 °C for an [Im]/[HTFSI] = 8/2 composition. The scan rate is 10 mV/s.

current. Furthermore, evolution of gas (H_2) was confirmed as bubbles at the cathode. This is indicative of the following phenomenon, occurring at the anode, electrolyte, and cathode:

$$\text{anode: } H_2 + 2\text{Im} \rightarrow 2\text{HIm}^+ + 2e^-$$

$$\text{electrolyte: proton conduction}$$

$$\text{cathode: } 2\text{HIm}^+ + 2\,e^- \rightarrow 2\text{Im} + H_2$$

It is worthwhile to explore electrode reactions of base-rich Im/HTFSI compositions at the three-phase boundary of the composition/Pt/H_2 or O_2. Cyclic voltammetric behaviors of some Im/HTFSI compositions at 80 °C are shown in Figure 10. In these experiments, Pt and Pt-black electrodes immersed in the compositions worked as working (WE) and counter (CE) electrodes, respectively, and a Pt electrode with H_2 bubbling as a reference electrode (RE). The cell potential was scanned from the open circuit potential (OCP) to −0.1 V for the first scan followed by scanning to +1.5 V and finally to the OCP. When the working electrode is in an Ar atmosphere, the voltammograms show remarkable reduction and oxidation currents at around 0 V. For each composition, the reduction currents could be observed from ca. 0 V followed by oxidation currents due to reoxidation of the reduced species. The redox potential was ca. 0 V with observation of gas bubbles on the WE in the reduction process. The potential of 0 V, therefore, corresponds to the hydrogen redox potential, and the RE can be considered as a reversible hydrogen electrode (RHE). Im/HTFSI compositions and H_2 are electroactive with Pt, and the electrochemical equilibrium reached at the reference electrode is

$$2\text{HIm}^+ + 2e^- \rightleftarrows 2\text{Im} + H_2$$

Thus, the reduction currents at negative potential are from H_2 evolution from the compositions, and the following oxidation currents result from the reoxidation of the evolved H_2. We could not observe adsorption/desorption of H_2 on/from a Pt surface as well as Pt oxidation/reduction, as seen in a H_2SO_4 aqueous solution.[89] It is worth mentioning that the Im-rich compositions exhibit activity with a Pt electrode under a H_2 atmosphere, and

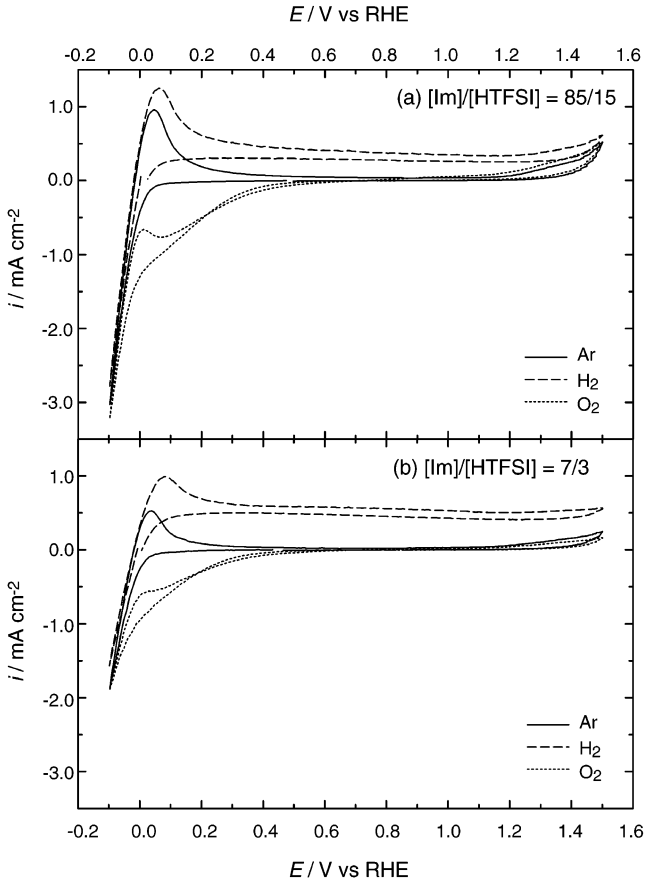

Figure 10. Cyclic voltammograms for [Im]/[HTFSI] = (a) 85/15 and (b) 7/3 compositions at 80 °C. The scan rate is 50 mV/s. WE is a Pt wire in an Ar, a H_2, or an O_2 atmosphere. CE is a Pt-black wire, and RE is a Pt wire in a H_2 atmosphere.

the HIm^+ is a candidate for an electroactive component. Besides the proton redox behavior, irreversible oxidation currents at potentials over 1.2 V for all compositions, especially in the [Im]/[HTFSI] = 85/15 composition, could also be observed.

Upon a change in the working atmosphere from Ar to H_2, the results of cyclic voltammograms apparently changed as shown in Figure 10. Large diffusion-limiting oxidation currents were detected after the reoxidation for [Im]/[HTFSI] = 85/15 and 7/3 compositions. The H_2 oxidation on the Pt working electrode gave rise to the oxidation currents. The H_2 bubbles could be visually observed on the counter electrode. We consider these results to be comprehensible and decisive evidence of the proton conduction for these compositions. In Im excess compositions, the conductivity shows a high value, and the fast proton transport is confirmed by NMR measurements. In addition, the proton conduction is identified by direct current polarization in a H_2 atmosphere.

When the working electrode is under an O_2 bubbling atmosphere, a radical change in the shapes of the cyclic voltammograms, as shown in Figure 10, is observed. The cathodic current is observed at a potential below 0.8 V vs RHE, and the waves, corresponding to the evolution and reoxidation of H_2, are overlapped below 0 V vs RHE. The cathodic current, judged from the potential, appears to be assigned to the 4-electron O_2 reduction reaction

$$O_2 + 4H^+ + 4e^- \rightarrow 2H_2O$$

At present, we cannot deny concurrent 2-electron O_2 reduction at a lower potential. Since the proton carrier in this system is

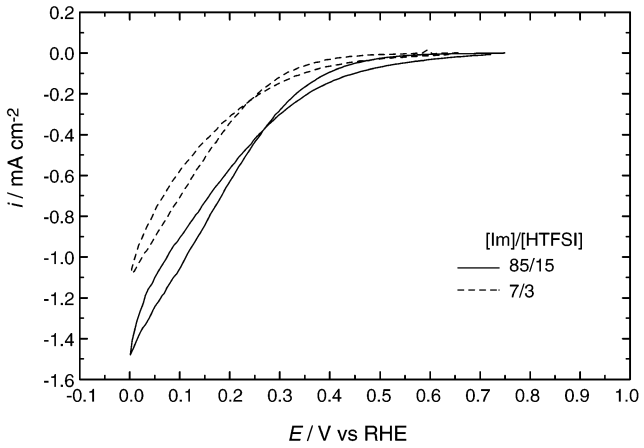

Figure 11. Cyclic voltammograms for [Im]/[HTFSI] = 85/15 and 7/3 compositions at 80 °C. WE is a Pt wire in an O_2 atmosphere. CE is a Pt-black wire in a H_2 atmosphere, and RE is a Pt wire in a H_2 atmosphere. The cell potential is scanned from OCP to 0 V for the first scan followed by scanning to the OCP successively, at 10 mV/s.

HIm^+, the reaction can be expressed as

$$O_2 + 4ImH^+ + 4e^- \rightarrow 2H_2O + 4Im$$

It should be noted that ImH^+ is active for the oxygen reduction. Although the overpotential of the oxygen reduction is rather large and the reaction kinetics is slow, this finding is quite promising for the use of base-rich Im/HTFSI compositions as electrolytes of a fuel cell under nonhumidifying conditions.

Fuel Cell Test under Nonhumidifying Conditions. Figure 11 shows cyclic voltammograms of base-rich Im/HTFSI compositions, where the working and counter electrodes are under O_2 and H_2 bubbling atmospheres. These represent current vs potential (vs RHE) characteristics of H_2/O_2 fuel cells under nonhumidifying conditions. Although the potential drop with increasing current density is apparent, this is, to our knowledge, the first evidence of electric power generation by a H_2/O_2 fuel cell using Brønsted acid−base ionic liquids as proton-conducting nonaqueous electrolytes. In the present fuel cell system, the Im molecule functions not only as a proton carrier like water in the acidic electrolytes but also as a H^+ donor and an acceptor for O_2 reduction and H_2 oxidation reactions, respectively. Proton conduction by structure diffusion (Grotthuss mechanism) involves intermolecular proton transfer and structural reorganization by hydrogen bond breaking and forming processes.[76−77,84,90] For prolonged cycling of the potential, the current gradually decreased, possibly due to adsorption of Im onto the electrode surface. However, numerous combinations are possible for Brønsted acid−base ionic liquids. We have already found other proton-conducting ionic liquids of this variety, details of which will be reported elsewhere. The concept of an ionic liquid may be used with compatible polymers for the construction of solid-state proton conductors, and further, an acidic site and/or a basic site can be affixed to a polymer backbone. This finding may open up a new field of fuel cells under nonhumidifying conditions, which may be operated at elevated temperature above 100 °C.

Summary and Conclusion

Im and HTFSI were mixed at various molar ratios. The composition at the equivalent molar ratio formed a neutral salt with a congruent melting point of 73 °C. There is a eutectic with a melting point of −6 °C for compositions between pure HTFSI and the equimolar salt, and also between the equimolar salt and imidazole at 6 °C. Some of the compositions with certain molar ratios of Im and HTFSI were liquid at room temperature. The analyses of the conductivity, ^1H NMR chemical shift, self-diffusion coefficient, and electrochemical polarization results indicate that the proton conduction in the Im−HTFSI system depends on the composition, and in Im-rich compositions it follows a combination of Grotthuss- and vehicle-type mechanisms. With excess Im in the compositions, fast proton exchange reactions between the protonated Im cation and Im could be envisaged. The base-rich Im/HTFSI compositions are electroactive for both H_2 oxidation and O_2 reduction at the Pt electrode. The activity of the components is a very significant factor to consider in operating a fuel cell, and the fast proton conduction is also a requisite to restrain IR drop of the electrolyte. Furthermore, the durability of oxidation of electrolytes at an oxygen reduction potential cannot be ignored. However, with an increase in the fraction of protonated Im, HIm^+, the oxidation stability is greatly enhanced, and the protic ionic liquid exhibits excellent thermal stability as a neutral ionic liquid. The thermally stable neutral salt as well as other compositions is, therefore, a new candidate for proton conductors, while H_2 gas diffusion must not be neglected since the solubility of gases in ILs is generally high.[2f,91] We have, therefore, focused our attention on constructing solid-state proton conductors using polymers based on the concept of ionic liquids. A radical polymerization of a vinyl monomer in the Im-rich compositions following a method described in our earlier paper was conducted.[17] The obtained polymer electrolytes were transparent and exhibited moderately high ionic conductivity. This is a simple approach, and proper modification may open a route to obtain a highly proton conducting polymer electrolyte, with sufficiently high mechanical strength. The Brønsted acid−base ionic liquid system is, therefore, a new candidate for a proton conductor for operation under nonhumidifying conditions and at elevated temperature.

Acknowledgment. This research was supported in part by a Grant-in-Aid for Scientific Research on Priority Area "Molecular Synchronization for Design of New Materials System (no. 404/11167234)" from the Japanese Ministry of Education, Science, Sports, and Culture and by the Technology Research Grant Program in 2001 from NEDO of Japan. In addition, we appreciate the supply of HTFSI from Morita Chemical Industries.

References and Notes

(1) (a) Cooper, E. I.; Sullivan, E. J. M. In *Molten salts VIII*; Gale, R. J., Blomgren, G., Kojima, H., Eds.; The Electrochemical Society Proceedings Series; Electrochemical Society: Pennington, NJ, 1992; Vol. 92-16, p 386. (b) Wilkes, J. S.; Zaworotko, M. J. *J. Chem. Soc., Chem. Commun*. **1992**, 965.

(2) (a) Olivier, H. *J. Mol. Catal*. **1999**, *146*, 285. (b) Welton, T. *Chem. Rev*. **1999**, *99*, 2071. (c) Holbrey, J. D.; Seddon, K. R. *Clean Prod. Process*. **1999**, *1*, 223. (d) Wasserscheid, P.; Keim, W. *Angew. Chem., Int. Ed*. **2000**, *39*, 3772. (e) Gordon, C. M. *Appl. Catal*. **2001**, *222*, 101. (f) Sheldon, R. *Chem. Commun*. **2001**, 2399.

(3) (a) Seddon, K. R. *J. Chem. Technol. Biotechnol*. **1997**, *68*, 351. (b) Blanchard, L. A.; Hancu, D.; Beckman, E. J.; Brennecke, J. F. *Nature* **1999**, *399*, 28. (c) Earle, M. J.; Seddon, K. R. *Pure Appl. Chem*. **2000**, *72*, 1391. (d) Adam, D. *Nature* **2000**, *407*, 938.

(4) Carlin, R. T.; De Long, H. C.; Fuller, J.; Trulove, P. C. *J. Electrochem. Soc*. **1994**, *141*, L73.

(5) Fuller, J.; Carlin, R. T.; Osteryoung, R. A. *J. Electrochem. Soc*. **1997**, *144*, 3881.

(6) Sun, J.; Forsyth, M.; MacFarlane, D. R. *J. Phys. Chem. B* **1998**, *102*, 8858.

(7) MacFarlane, D. R.; Meakin, P.; Sun, J.; Amini, N.; Forsyth, M. *J. Phys. Chem. B* **1999**, *103*, 4164.

(8) (a) Matsumoto, H.; Yanagida, M.; Tanimoto, K.; Nomura, M.; Kitagawa, Y.; Miyazaki, Y. *Chem. Lett*. **2000**, 922. (b) Matsumoto, H.; Matsuda, T.; Miyazaki, Y. *Chem. Lett*. **2000**, 1430.

(9) Nanjundiah, C.; McDevitt, S. F.; Koch, V. R. *J. Electrochem. Soc*. **1997**, *144*, 3392.

(10) (a) Koch, V. R.; Dominey, L. A.; Nanjundiah, C. *J. Electrochem. Soc*. **1996**, *143*, 798. (b) McEwen, A. B.; McDevitt, S. F.; Koch, V. R. *J. Electrochem. Soc*. **1997**, *144*, L84. (c) McEwen, A. B.; Ngo, H. L.; LeCompte, K.; Goldman, J. L. *J. Electrochem. Soc*. **1999**, *146*, 1687.

(11) Suarez, P. A. Z.; Selbach, V. M.; Dullius, J. E. L.; Einloft, S.; Piatnicki, C. M. S.; Azambuja, D. S.; de Souza, R. F.; Dupont, J. *Electrochim. Acta* **1997**, *42*, 2533.

(12) Hagiwara, R.; Ito, R. *J. Fluorine Chem.* **2000**, *105*, 221.

(13) (a) O'Regan, B.; Grätzel, M. *Nature* **1991**, *353*, 737. (b) Hagfeldt, A.; Grätzel, M. *Chem. Rev.* **1995**, *95*, 49.

(14) (a) Papageorgiou, N.; Athanassov, Y.; Armand, M.; Bonhôte, P.; Pettersson, H.; Azam, A.; Grätzel, M. *J. Electrochem. Soc*. **1996**, *143*, 3099. (b) Kawano, R.; Watanabe, M. *Chem. Commun.* **2003**, 330.

(15) (a) Watanabe, M.; Yamada, S.; Ogata, N. *J. Chem. Soc., Chem. Commun.* **1993**, 929. (b) Fuller, J.; Breda, A. C.; Carlin, R. T. *J. Electrochem. Soc*. **1997**, *144*, L67. (c) Carlin, R. T.; Fuller, J. *Chem. Commun.* **1997**, 1345. (d) Fuller, J.; Breda, A. C.; Carlin, R. T. *J. Electroanal. Chem*. **1998**, *459*, 29.

(16) (a) Doyle, M.; Choi, S. K.; Proulx, G. *J. Electrochem. Soc*. **2000**, *147*, 34. (b) Sun, J.; Jordan, L. R.; Forsyth, M.; MacFarlane, D. R. *Electrochim. Acta* **2001**, *46*, 1703.

(17) Noda, A.; Watanabe, M. *Electrochim. Acta* **2000**, *45*, 1265.

(18) (a) Ohno, H.; Ito, K. *Chem. Lett*. **1998**, 751. (b) Yoshizawa, M.; Ohno, H. *Electrochim. Acta* **2001**, *46*, 1723.

(19) Fuller, J.; Carlin, R. T.; De Long, H. C.; Haworth, D. *J. Chem. Soc., Chem. Commun*. **1994**, 299.

(20) Koch, V. R.; Nanjunduah, C.; Appetecchi, G. B.; Scrosati, B. *J. Electrochem. Soc*. **1995**, *142*, L116. (b) Croce, F.; D'Aprano, A.; Nanjundiah, C.; Koch, V. R.; Walker, C. W.; Salmon, M. *J. Electrochem. Soc*. **1996**, *143*, 154.

(21) (a) Chauvin, Y.; Olivier-Bourbigou, H. *CHEMTECH* **1995**, 26. (b) Chauvin, Y.; Mussmann, L.; Olivier, H. *Angew. Chem., Int. Ed. Engl.* **1995**, *34*, 2698.

(22) Suarez, P. A. Z.; Dullius, J. E. L.; Einloft, S.; de Souza, R. F.; Dupont, J. *Polyhedron* **1996**, *15*, 1217.

(23) Bonhôte, P.; Dias, A.-P.; Papageorgiou, N.; Kalyanasundaram, K.; Grätzel, M. *Inorg. Chem*. **1996**, *35*, 1168.

(24) (a) Bowlas, C. J.; Bruce, D. W.; Seddon, K. R. *Chem. Commun.* **1996**, 1625. (b) Gordon, C. M.; Holbrey, J. D.; Kennedy, A. R.; Seddon, K. R. *J. Mater. Chem.* **1998**, *8*, 2627.

(25) Golding, J. J.; MacFarlane, D. R.; Spiccia, L.; Forsyth, M.; Skelton, B. W.; White, A. H. *Chem. Commun.* **1998**, 1593.

(26) Hagiwara, R.; Hirashige, T.; Tsuda, T.; Ito, Y. *J. Fluorine Chem.* **1999**, *99*, 1.

(27) Holbrey, J. D.; Seddon, K. R. *J. Chem. Soc., Dalton Trans.* **1999**, 2133.

(28) Larsen, A. S.; Holbrey, J. D.; Tham, F. S.; Reed, C. A. *J. Am. Chem. Soc.* **2000**, *122*, 7264.

(29) Hirao, M.; Sugimoto, H.; Ohno. *J. Electrochem. Soc*. **2000**, *147*, 4168.

(30) Merrigan, T. L.; Bates, E. D.; Dorman, S. C.; Davis, J. H., Jr. *Chem. Commun.* **2000**, 2051.

(31) Lall, S. I.; Mancheno, D.; Castro, S.; Behaj, V.; Cohen, J.-L. I.; Engel, R. *Chem. Commun.* **2000**, 2413.

(32) Ngo, H. L.; LeCompte, K.; Hargens, L.; McEwen, A. B. *Thermochim. Acta* **2000**, *357*−*358*, 97.

(33) (a) Velázquez, C. S.; Hutchison, J. E.; Murray, R. W. *J. Am. Chem. Soc.* **1993**, *115*, 7896. (b) Terrill, R. H.; Hatazawa, T.; Murray, R. W. *J. Phys. Chem. B* **1995**, *99*, 16676. (c) Williams, M. E.; Murray, R. W. *J. Phys. Chem. B* **1999**, *103*, 10221. (d) Leone, A. M.; Weatherly, S. C.; Williams, M. E.; Thorp, H. H.; Murray, R. W. *J. Am. Chem. Soc.* **2001**, *123*, 218.

(34) Yoshizawa, M.; Hirao, M.; Ito-Akita, K.; Ohno, H. *J. Mater. Chem.* **2001**, *11*, 1057.

(35) Golding, J. J.; Hamid, N.; MacFarlane, D. R.; Forsyth, M.; Forsyth, C.; Collins, C.; Huang, J. *Chem. Mater*. **2001**, *13*, 558.

(36) Yoshizawa, M.; Ogihara, W.; Ohno, H. *Electrochem. Solid State Lett.* **2001**, *4*, E25.

(37) Matsumoto, H.; Kitagawa, Y.; Miyazaki, Y. *Chem. Lett*. **2001**, 182.

(38) Armstrong, D. W.; Zhang, L.-K.; He, L.; Gross, M. L. *Anal. Chem.* **2001**, *73*, 3679.

(39) MacFarlane, D. R.; Golding, J. J.; Forsyth, S.; Forsyth, M.; Deacon, G. B. *Chem. Commun.* **2001**, 1430.

(40) Dzyuba, S. V.; Bartsch, R. A. *Chem. Commun.* **2001**, 1466.

(41) Brown, R. J. C.; Dyson, P. J.; Ellis, D. J.; Welton, T. *Chem. Commun.* **2001**, 1862.

(42) Abbott, A. P.; Capper, G.; Davies, D. L.; Munro, H. L.; Rasheed, R. K.; Tambyrajah, V. *Chem. Commun.* **2001**, 2010.

(43) Pernak, J.; Czepukowicz, A.; Poźniak, R. *Ind. Eng. Chem. Res.* **2001**, *40*, 2379.

(44) Visser, A. E.; Holbrey, J. D.; Rogers, R. D. *Chem. Commun*. **2001**, 2484.

(45) Suarez, P. A. Z.; Einloft, S.; Dullius, J. E. L.; de Souza, R. F.; Dupont, J. *J. Chim. Phys.* **1998**, *95*, 1626.

(46) (a) Huddleston, J. G.; Willauer, H. D.; Swatloski, R. P.; Visser, A. E.; Rogers, R. D. *Chem. Commun.* **1998**, 1765. (b) Visser, A. E.; Swatloski, R. P.; Reichert, W. M.; Griffin, S. T.; Rogers, R. D. *Ind. Eng. Chem. Res.* **2000**, *39*, 3596.

(47) Armstrong, D. W.; He, L.; Liu, Y.-S. *Anal. Chem.* **1999**, *71*, 3873.

(48) (a) Gannon, T. J.; Law, G.; Watson, P. R. *Langmuir* **1999**, *15*, 8429. (b) Law, G.; Watson, P. R.; Carmichael, A. J.; Seddon, K. R. *Phys. Chem. Chem. Phys.* **2001**, *3*, 2879. (c) Law, G.; Watson, P. R. *Langmuir* **2001**, *17*, 6138. (d) Law, G.; Watson, P. R. *Chem. Phys. Lett.* **2001**, *345*, 1.

(49) Seddon, K. R.; Stark, A.; Torres, M.-J. *Pure Appl. Chem.* **2000**, *72*, 2275.

(50) Kosmulski, M.; Osteryoung, R. A.; Ciszkowska, M. *J. Electrochem. Soc.* **2000**, *147*, 1454.

(51) (a) Wadhawan, J. D.; Schröder, U.; Neudeck, A.; Wilkins, S. J.; Compton, R. G.; Marken, F.; Consorti, C. S.; de Souza, R. F.; Dupont, J. *J. Electroanal. Chem.* **2000**, *493*, 75. (b) Schröder, U.; Wadhawan, J. D.; Compton, R. G.; Marken, F.; Suarez, P. A. Z.; Consorti, C. S.; de Souza, R. F.; Dupont, J. *New J. Chem.* **2000**, *24*, 1009.

(52) Katayama, Y.; Dan, S.; Miura, T.; Kishi, T. *J. Electrochem. Soc.* **2001**, *148*, C102.

(53) Carmichael, A. J.; Seddon, K. R. *J. Phys. Org. Chem.* **2000**, *13*, 591.

(54) Aki, S. N. V. K.; Brennecke, J. F.; Samanta, A. *Chem. Commun.* **2001**, 413.

(55) Baker, S. N.; Baker, G. A.; Kane, M. A.; Bright, F. V. *J. Phys. Chem. B* **2001**, *105*, 9663.

(56) (a) Wasserscheid, P.; Gordon, C. M.; Hilgers, C.; Muldoon, M. J.; Dunkin, I. R. *Chem. Commun.* **2001**, 1186. (c) Muldoon, M. J.; Gordon, C. M.; Dunkin, I. R. *J. Chem. Soc., Perkin Trans. 2* **2001**, 433.

(57) (a) Fletcher, K. A.; Storey, I. K.; Hendricks, A. E.; Pandey, S.; Pandey, S. *Green Chem.* **2001**, *3*, 210. (b) Fletcher, K. A.; Pandey, S.; Storey, I. K.; Hendricks, A. E.; Pandey, S. *Anal. Chim. Acta* **2001**, *21680*, 1.

(58) Every, H.; Bishop, A. G.; Forsyth, M.; MacFarlane, D. R. *Electrochim. Acta* **2000**, *45*, 1279.

(59) Huang, J.-F.; Chen, P.-Y.; Sun, I.-W. Wang, S. P. *Inorg. Chim. Acta* **2001**, *320*, 7.

(60) Noda, A.; Hayamizu, K.; Watanabe, M. *J. Phys. Chem. B* **2001**, *105*, 4603.

(61) Wong, D. S. H.; Chen, J. P.; Chang, J. M.; Chou, C. H. *Fluid Phase Equilib.* **2002**, *4954*, 1.

(62) Anthony, J. L.; Maginn, E. J.; Brennecke, J. F. *J. Phys. Chem. B* **2001**, *105*, 10942.

(63) Cammarata, L.; Kazarian, S. G.; Salter, P. A.; Welton, T. *Phys. Chem. Chem. Phys.* **2001**, *3*, 5192.

(64) Kazarian, S. G.; Briscoe, B. J.; Welton, T. *Chem. Commun.* **2000**, 1186.

(65) (a) Blanchard, L. A.; Brennecke, J. F. *Ind. Eng. Chem. Res.* **2000**, *40*, 287. (b) Blanchard, L. A.; Gu, Z.; Brennecke, J. F. *J. Phys. Chem. B* **2001**, *105*, 2437.

(66) Liu, F.; Abrams, M. B.; Baker, R. T.; Tumas, W. *Chem. Commun.* **2001**, 433.

(67) Gordon, C. M.; McLean, A. J. *Chem. Commun.* **2000**, 1395.

(68) Behar, D.; Gonzalez, C.; Neta, P. *J. Phys. Chem. A* **2001**, *105*, 7607.

(69) Marcinek, A.; Zielonka, J.; G_bicki, J.; Gordon, C. M.; Dunkin, I. R. *J. Phys. Chem. A* **2001**, *105*, 9305.

(70) Christie, S.; Subramanian, S.; Wang, L.; Zaworotko, M. J. *Inorg. Chem.* **1993**, *32*, 5415.

(71) Walden, P. *Bull. Acad. Imper. Sci. (St. Petersburg)* **1914**, 1800.

(72) Takahashi, T.; Tanase, S.; Yamamoto, O.; Yamauchi, S. *J. Solid State Chem.* **1976**, *17*, 353.

(73) (a) Wainright, J. S.; Wang, J.-T.; Weng, D.; Savinell, R. F.; Litt, M. *J. Electrochem. Soc*. **1995**, *142*, L121. (b) Samms. S. R.; Wasmus, S.; Savinell, R. F. *J. Electrochem. Soc*. **1996**, *143*, 1225. (c) Fontanella, J. J.; Wintersgill, M. C.; Wainright, J. S.; Savinell, R. F.; Litt, M. *Electrochim. Acta* **1998**, *43*, 1289. (d) Bouchet, R.; Siebert, E. *Solid State Ionics* **1999**, *118*, 287.

(74) (a) Donoso, P.; Gorecki, W.; Berthier, C.; Defendini, F.; Poinsignon, C.; Armand, M. B. *Solid State Ionics* **1988**, *28*−*30*, 969. (b) Gupta, P. N.; Singh, K. P. *Solid State Ionics* **1996**, *86*−*88*, 319. (c) Stevens, J. R.; Wieczorek, W.; Raducha, D.; Jeffrey, K. R. *Solid State Ionics* **1997**, *97*, 347. (d) Bozkurt, A.; Ise, M.; Kreuer, K. D.; Meyer, M. H.; Wegner, G. *Solid State Ionics* **1999**, *125*, 225. (e) Zukowska, G.; Rogowska, M.; Węczkowska, E.; Wieczorek, W. *Solid State Ionics* **1999**, *119*, 289. (f)

Zukowska, G.; Chojnacka, N.; Wieczorek, W. *Chem. Mater*. **2000**, *12*, 3578. (g) Bozkurt, A.; Meyer, M. H. *Solid State Ionics* **2001**, *138*, 259.

(75) (a) Casciola, M.; Costantino, U.; Marmottini, F. *Solid State Ionics* **1989**, *35*, 67. (b) Casciola, M.; Chieli, S.; Costantino, U.; Peraio, A. *Solid State Ionics* **1991**, *46*, 53. (c) Casciola, M.; Costantino, U.; Calevi, A. *Solid State Ionics* **1993**, *61*, 245.

(76) Kreuer, K. D.; Fuchs, A.; Ise, M.; Spaeth, M.; Maier, J. *Electrochim. Acta* **1998**, *43*, 1281.

(77) Kreuer, K. D. *Solid State Ionics* **1997**, *94*, 55.

(78) (a) Schuster. M.; Meyer, M. H.; Wegner, G.; Herz, H. G.; Ise, M.; Schuster. M.; Kreuer, K. D.; Maier, J. *Solid State Ionics* **2001**, *145*, 85. (b) Kreuer, K. D. *J. Membr. Sci.* **2001**, *185*, 29.

(79) (a) Hayamizu, K.; Aihara, Y.; Arai, S.; Price, W. S. *Solid State Ionics* **1998**, *107*, 1. (b) Hayamizu, K.; Aihara, Y.; Arai, S.; Martinez, C. G. *J. Phys. Chem. B* **1999**, *103*, 519. (c) Aihara, Y.; Sugimoto, K.; Price, W. S. Hayamizu, K. *J. Chem. Phys.* **2000**, *113*, 1981. (d) Hayamizu, K.; Aihara, Y.; Price, W. S. *J. Chem. Phys.* **2000**, *113*, 4785.

(80) (a) Stejskal, E. O. *J. Chem. Phys*. **1965**, *43*, 3597. (b) Price, W. S. *Concepts Magn. Reson.* **1997**, 9, 299. (c) Price, W. S. *Concepts Magn. Reson.* **1998**, *10*, 197.

(81) Kawada, A.; McGhie, A. R.; Labes, M. M. *J. Chem. Phys.* **1970**, *52*, 3121.

(82) (a) Foropoulos, J., Jr.; DesMarteau, D. D. *Inorg. Chem*. **1984**, *23*, 3720. (b) Haas, A.; Klare, Ch.; Betz, P.; Bruckmann, J.; Krüger, C.; Tsay, Y.-H.; Aubke, F. *Inorg. Chem.* **1996**, *35*, 1918.

(83) (a) Wilkes, J. S.; Levinsky, J. A.; Wilson, R. A.; Hussey, C. L. *Inorg. Chem*. **1982**, *21*, 1263. (b) Fannin, A. A., Jr.; Floreani, D. A.; King, L. A.; Landers, J. S.; Piersma, B. J.; Stech, D. J.; Vaughn, R. L.; Wilkes, J. S.; Williams, J. L. *J. Phys. Chem.* **1984**, *88*, 2614. (c) Sanders, J. R.; Ward, E. H.; Hussey, C. L. *J. Electrochem. Soc*. **1986**, *133*, 325.

(84) (a) Joop, N.; Zimmermann, H. *Ber. Bunsen-Ges. Phys. Chem*. **1962**, *66*, 440. (b) Ralph, E. K.; Grunwald, E. *J. Am. Chem. Soc.* **1968**, *90*, 517. (c) Daycock, J. T.; Jones, G. P.; Evans, J. R. N.; Thomas, J. M. *Nature* **1968**, *218*, 671. (d) Glasser, L. *Chem. Rev.* **1975**, *75*, 5. 21. (e) Brédas, J. L.; Poskin, M. P.; Delhalle, J.; André, J. M.; Chojnacki, H. *J. Phys. Chem.* **1984**, *88*, 5882. (f) Scheiner, S.; Yi, M. *J. Phys. Chem.* **1996**, *100*, 9235. (g) Münch, W.; Kreuer, K. D.; Silvertri, W.; Maier, J.; Seifert, G. *Solid State Ionics* **2001**, *145*, 437.

(85) Kreuer, K. D.; Rabenau, A.; Weppner, W. *Angew. Chem., Int. Ed. Engl*. **1982**, *21*, 208.

(86) Kreuer, K. D. *Chem. Mater*. **1996**, *8*, 610.

(87) Koppel, I. A.; Taft, R. W.; Anvia, F.; Zhu, S.-Z. Hu, L.-Q.; Sung, K.-S.; DesMarteau, D. D.; Yagupolskii, L. M.; Yagupolskii, Y. L.; Ignat'ev, N. V.; Kondratenko, N. V.; Volkonskii, A. Y.; Vlasov, V. M.; Notario, R.; Maria, P. C. *J. Am. Chem. Soc.* **1994**, *116*, 3047.

(88) Dippel, Th.; Kreuer, K. D.; Lassègues, J. C.; Rodriguez, D. *Solid State Ionics* **1993**, *61*, 41.

(89) Sawyer, D. T.; Roberts, J. L., Jr. *Experimental Electrochemistry for Chemists*; John Wiley: New York, 1947; p 67.

(90) Kreuer, K. D. *Solid State Ionics* **2000**, *136*−*137*, 149.

(91) (a) Suarez, P. A. Z.; Dullius, J. E. L.; Einloft, S.; de Souza, R. F.; Dupont, J. *Polyhedron* **1996**, *15*, 1217. (b) Suarez, P. A. Z.; Dullius, J. E. L.; Einloft, S.; de Souza, R. F.; Dupont, J. *Inorg. Chim. Acta* **1997**, *255*, 207. (c) Monterio, A. L.; Zinn, F. K.; de Souza, R. F.; Delgado, M. R.; Dupont, J. *Tetrahedron: Asymmetry* **1997**, *8*, 177. (d) Berger, A.; de Souza, R. F.; Delgado, M. R.; Dupont, J. *Tetrahedron: Asymmetry* **2001**, *12*, 1825.